JOURNAL OF MATERIALS SCIENCE **35** (2000) 3373–3382

Microstructural assessment of laser nitrided Ti-6Al-4V alloy

H. XIN, C. HU, T. N. BAKER
Metallurgy and Engineering Materials Group, Department of Mechanical Engineering, University of Strathclyde, Glasgow G1 U.K.
E-mail: tnb@mecheng.strath.ac.uk

A microstructural study of the phases developed during the laser nitriding of a Ti-6Al-4V alloy by, using a CL5 continuous CO_2 laser with a spinning beam and concentration of 80% nitrogen, was undertaken. The vertical sections, perpendicular to the melt track were examined by optical microscopy and scanning electron microscopy (SEM), while specimens for X-ray diffractometry (XRD), X-ray photospectroscopy (XPS) and transmission electron microscopy/selected area electron diffraction (TEM/SAED), were taken parallel to the melt track. In this way the variation in microstructure as a function of depth from the laser treated surface, was studied. This supplemented XRD and XPS investigations undertaken previously. Two zones were identified. Zone 1, within 50 μm of the surface, contained well defined dendrites of fcc $TiN_{0.8}$, plus hcp $TiN_{0.3}$ and hcp α'Ti. Zone 2, below 50 μm, consisted of needles of hcp α'Ti. From a consideration of the hardness profiles in Zone 2, it is suggested that at the top of the zone, the α' phase is, in fact, a solid solution containing 3–4% N, which decreased to $<$1% N at the bottom of the zone. The TEM/SAED study permitted the three phases fcc $TiN_{0.8}$, hcp $TiN_{0.3}$ and hcp α'Ti to be identified through a combination of morphology and SAED patterns. This also showed that the fcc$TiN_{0.8}$ contained fringes, which were considered to be stacking fault fringes and allowed this phase to be readily recognized in the TEM. The presence of stacking faults may be associated with the high nitrogen concentration of 80% used for the laser nitriding in this work.

1. Introduction

Although several surface nitriding treatments based on titanium nitride, such as plasma nitriding or PVD coating, are commercially available for titanium alloys, all these processes are carried out in the solid state and the depth of coating and therefore hardening is restricted by the low rate of nitrogen diffusivity. The diffusion coefficient of nitrogen in titanium is more than a thousand times lower than that in steels [1]. In order to achieve the depth of hardening required to produce protection against erosion or abrasive wear, which is normally regarded as 0.5–1.0 mm, it is necessary to alloy the titanium surface in the molten state. This depth of surface hardening can readily be achieved by laser melting the surface in the presence of nitrogen. Laser nitriding titanium alloys results in non-equilibrium structures in the melt zone and it is to be expected that the high temperature phases indicated on the equilibrium diagram, will be quenched-in, due to the very high cooling rates. Therefore nitrogen may well be retained in solid solution during solidification and cooling to room temperature [2]. Laser nitriding of titanium alloys has been the subject of investigation for over 15 years [3–9]. The aim has been to produce a nitrided surface giving improved tribological properties. Few detailed studies of the microstructure have been undertaken, since complex microstructures are developed in the solidified melt zone and ion milling techniques are necessary to produce high quality foils for TEM examination. The properties of the surface layer depend to an extent on the size and morphology of the hard fcc TiN_x, its chemical nature and volume fraction. The amount of TiN_x formed is dependent on the surface to volume ratio of the melt pool, on the interaction time and the nitrogen concentration in the environment [8, 9].

Recent work [11,12] using XRD and XPS techniques has shown that in a laser nitrided Ti-6Al-4V specimen processed using 2.8 kW laser power, 0.25 mm radius beam, 10 mm s^{-1} traverse velocity, 80% nitrogen concentration and a spinning beam, the large dendritic features which formed about 50 μm below the surface, [Zone 1] had a composition of $TiN_{0.8}$ in the top surface and $TiN_{0.85}$ at a depth of 35 μm. Also in this layer, $TiN_{0.3}$ and α'-Ti phases (probably with nitrogen in solid solution) were identified. The needle structure below 50 μm depth [Zone 2], was also α'-Ti, probably with nitrogen in solid solution.

Few studies using the TEM technique have been reported [e.g. 13–15], and most of the structural information in the literature has been obtained from X-ray measurements and SEM studies. However, almost all the results presented in these are papers concerned with

films deposited by PVD and CVD methods. To date, we are not aware of any detailed studies using TEM to describe the microstructure produced by the laser nitriding process. Although our previous work [11, 12] provided a tentative understanding of phases by using XRD and XPS techniques, the microstructures of the phases are not well established.

The specific objective of present work was to use the TEM technique to identify the different phases as a function of depth in the melt zone and to relate the results to those obtained by XRD and XPS studies. It was considered that by this approach, the optimisation of laser conditions to achieve improved wear resistance could be undertaken through knowledge of the microstructure.

2. Experimental procedure

Laser nitriding of single tracks was carried out at AEA Culham Laboratory, Abingdon, UK, using a 5 kW continuous (CL5) CO_2 laser with a spinning beam facility. A Ti-6Al-4V alloy was used as the base material in this investigation. The specimens were in the form of sheet $80 \times 40 \times 3$ mm. The operating parameters were 2.8 kW laser power, 0.25 mm radius beam, 10 mm s^{-1} traverse velocity, a spinning beam, and an 80% nitrogen + 20% argon gas mixture introduced at a flow rate of 50 l/min. The beam was spun to a diameter of 4 mm at 1500 rpm.

Thin foils were prepared by cutting slices (1 mm thick) from several different depths in the solidified melt zone parallel to the laser track, using a slitting wheel. The slices were ground mechanically to 250 μm from the side close to the heat-affected zone (HAZ) and without any grinding on the side close to the surface. Discs of 3 mm diameter were obtained from the slice by spark erosion. The grinding was then repeated, but only from the side close to the HAZ, to about 120 μm depth, and then to 220 μm and 440 μm, using SiC 1200 grade paper under a stream of cold water. The thin discs of the laser nitrided titanium alloys were dimpled from the side close to heat affected zone by means of a Gatan Model 656 Dimple Grinder. This was set at a load of 20 g. The polishing wheel used 2–4 μm diamond paste and was followed by a polishing cloth with 0.05 μm alumina. The dimpling side of the thin disc was first polished for about 5 minutes to clean the scratches left by the dimpling procedure. Only one side of the thin disc was ground to give a final thickness of 20 μm. Finally, the thin foils were prepared from the discs using the Gatan Model 691 Precision Ion Polishing System (PIPS^{TM}). This was set at a voltage of 5 keV, with a 4 degree angle of both guns at the start of milling and reduced to an angle of 2 degrees, when the specimen became transparent, as seen from the view window. Electron microscopy of thin foils was performed in a Philips EM 400T transmission electron microscope (TEM) at 120 kV.

3. Results

3.1. Optical and SEM microstructures

Our previous work [8, 11, 12, 16] has described the microstructures of laser nitrided titanium alloys processed using different laser conditions. Here, Fig. 1 shows optical and SEM micrographs of laser nitrided Ti-6Al-4V alloy processed with the conditions described in Section 2. It was found that the large dendritic layer formed at the surface (Zone 1), was about 50 μm in thickness. Below this layer, an intermediate layer about 350 μm in thickness, (Zone 2), comprised needle-like structures. The HAZ was then reached in these specimens.

3.2. XRD studies

In the present work, which is an extension of that published previously [11, 12], detailed XRD spectra of the laser nitrided Ti-6Al-4V specimen, from the top surface and at depths below the surface of 120, 220 μm (both in the melt zone) and 490 μm (in the HAZ), are shown in Figs 2 to 5. The points ■, ♦ and ● show the expected positions of the peaks for fcc TiN_x, $TiN_{0.3}$ and α-Ti respectively. It was found that a strong TiN_x peak appeared in the spectrum obtained from the top surface, Fig. 2. A very small TiN_x peak can be observed at a depth of 120 μm, Fig. 3, while it disappeared at the depths of 220 and 490 μm, Figs 4 and 5. The intensity of the $TiN_{0.3}$ peak is much weaker than that of the α'-Ti, peak, Fig. 2b. The above results indicate that TiN_x with some α'-Ti and very little $TiN_{0.3}$, were formed in Zone 1. The $TiN_{0.3}$ peak is not observed below 120 μm, and only the α'-Ti peak appeared, Figs 3–5. It is interesting to note that at a depth of 120 μm, the α'-Ti peak shifted to a smaller 2θ value than expected, Figs 2 and 3, and to a larger 2θ value than expected at a depth of 490 μm, Figs 4 and 5. This indicates that the lattice parameter data of α'-Ti is influenced by residual stresses, produced by the rapid cooling in the laser processing, and the nitrogen concentration in the melt zone.

The X-ray diffraction data, obtained from different depths, was treated by the least mean squares calculation to obtain the lattice parameters of TiN_x, $TiN_{0.3}$ and α'-Ti. The fcc TiN_x phase, which has an NaCl (f.c.c.) structure, has, at the stoichiometric composition, a lattice parameter of 4.240 A [17]. The previous XPS results [12] confirmed that the titanium nitride formed at the top surface had a composition of $TiN_{0.8}$, while the present results show that the lattice parameter of $TiN_{0.8}$ on the top surface is 4.225 A. The α'-Ti phase was formed throughout the melt zone, but had different lattice parameters. On the top surface, $a = 2.937$ A, $c = 4.709$ A, but these decreased to $a = 2.936$ A, $c = 4.702$ A, at a depth of 220 μm. Lengauer [18] has reported that a $TiN_{0.3}$ phase was formed near the nitrogen-rich phase boundary in the TiN/Ti mixture after arc melting, with lattice parameters of $a = 2.974$ A, $c = 4.792$ A. The XRD results in the present work show that the $TiN_{0.3}$ phase is formed only at the top surface layer (within the first 50 μm), that the quantity of $TiN_{0.3}$ is very small and just produces a (011) peak, but which was not of sufficient intensity to be used to calculate the lattice parameter. This phase is a non-equilibrium phase developed by the rapid solidification occurring during cooling following laser processing.

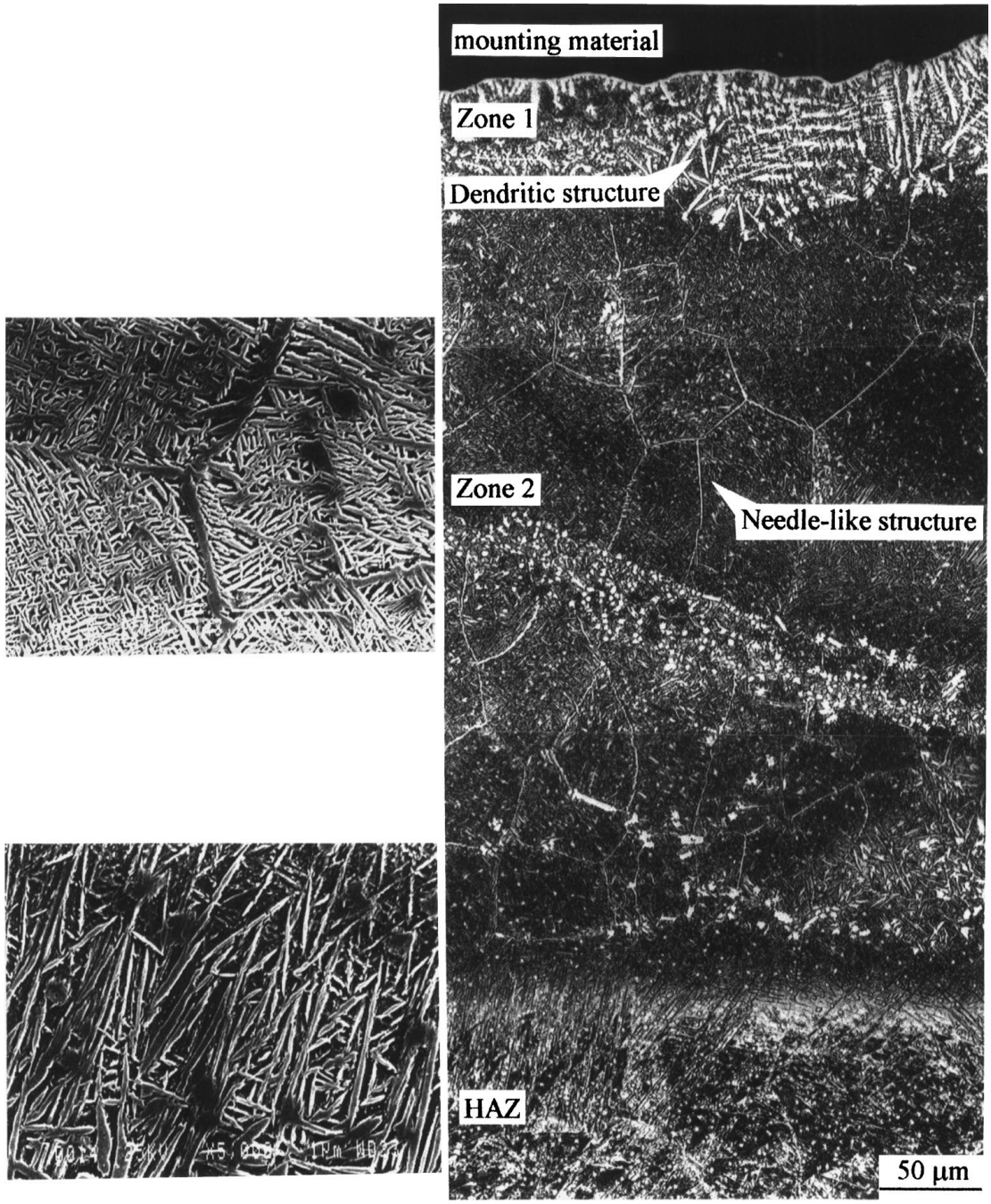

Figure 1 Optical and SEM micrographs of a vertical section of a laser nitrided specimen showing Zones 1 and 2.

3.3. Transmission electron microscopy

While SAED associated with TEM has an accuracy of only ±1%, and therefore cannot approach the accuracy of X-ray diffractometry, the ability to identify locally, small amounts of phases, is a key feature of the technique. Unfortunately this was not possible in an on-line mode in our system. Therefore it was essential to combine SAED patterns with bright/dark field images to use the morphology of the three main phases, fcc $TiN_{0.8}$, hcp $TiN_{0.3}$ and hcp α', identified earlier by XRD and XPS techniques, in the TEM identification of these phases. The fcc TiN identified using XRD, was always hypostoichiometric relative to nitrogen. TEM bright (BF) and dark (DF) field images of this phase, when tilted to the correct positions, invariably displayed fringe contrast. These are seen in Fig. 6. The large dendrites in this top surface BF image are compactly arranged, some exhibiting fringes, and the SAED pattern taken from position x, in Fig. 6a, and given in Fig. 6c, was indexed as fcc, with a [114] zone axis. The DF image was obtained using the 220 reflection.

An example of the identification of two phases from the same field of view is seen in Fig. 7. The BF image of the grain with the fringes, A in Fig. 7a, matches the centre of the DF (331 reflection) image in Fig. 7b, with the corresponding SAED from A in Fig. 7c. This was indexed as a [001] zone axis. When the aluminium ring pattern, seen in Fig. 7c A, was used for calibration, the SAED pattern was indexed as an fcc structure with a lattice parameter of 4.24 A, corresponding to TiN. The other two SAED patterns in Fig. 7c which were obtained following separate tilting experiments, were from positions C, a quasi spherical grain which showed no fringes, and B, the interface between A and C. These

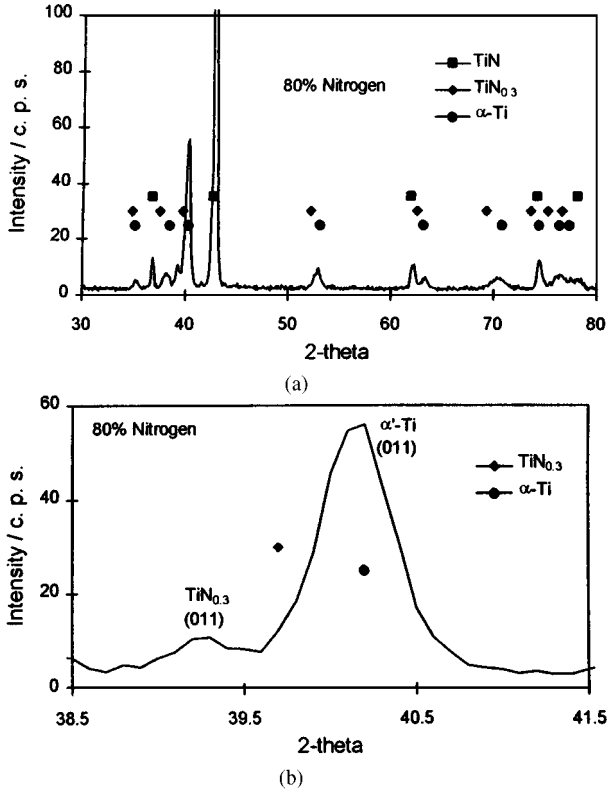

Figure 2 (a) X-Ray Diffraction Spectra from the top surface of a laser nitrided Ti alloy. (b) Details of (011) peaks of $TiN_{0.3}$ and α'Ti phases.

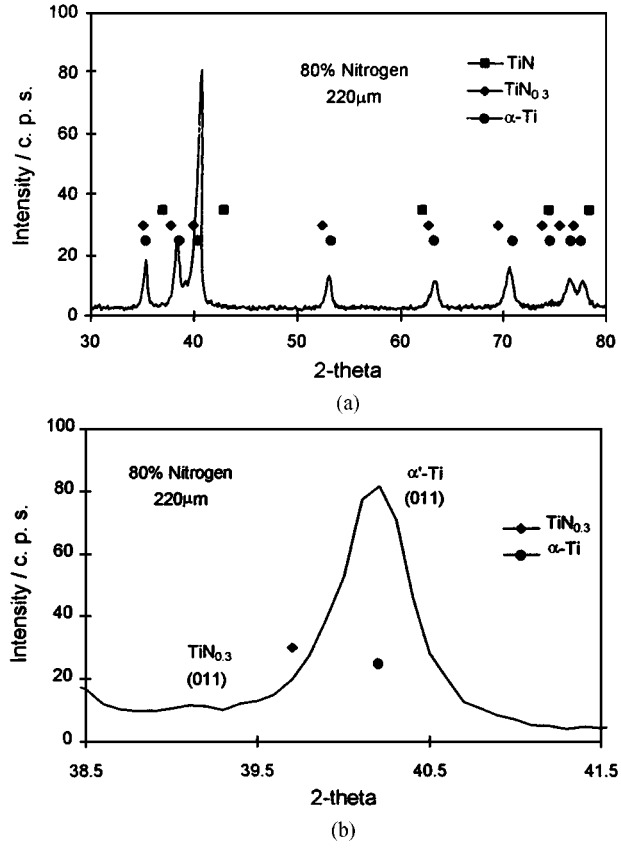

Figure 4 (a) X-Ray Diffraction Spectra at a depth of 220 μm of a laser nitrided Ti alloy. (b) Details of (011) peaks of $TiN_{0.3}$ and α'Ti phases.

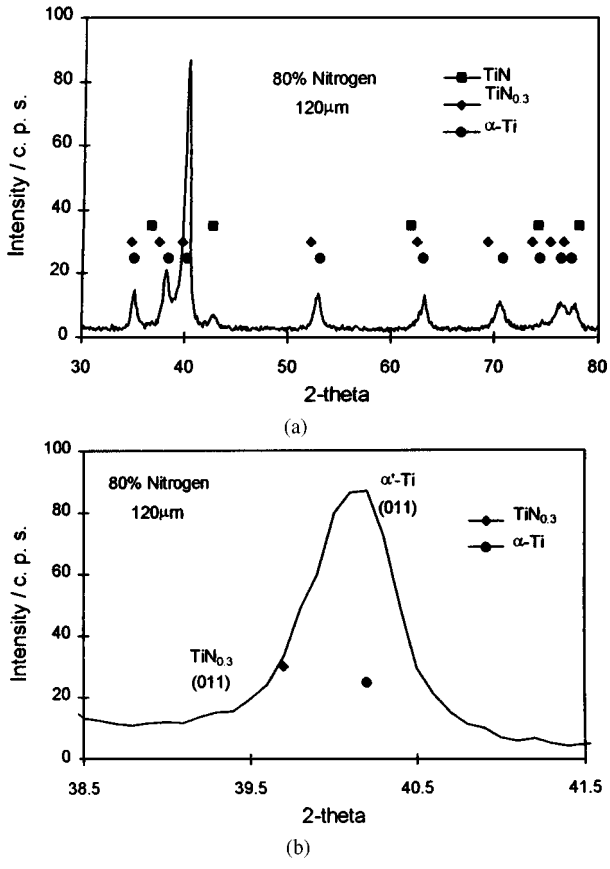

Figure 3 (a) X-Ray Diffraction Spectra at a depth of 120 μm of a laser nitrided Ti alloy. (b) Details of (011) peaks of $TiN_{0.3}$ and α'Ti phases.

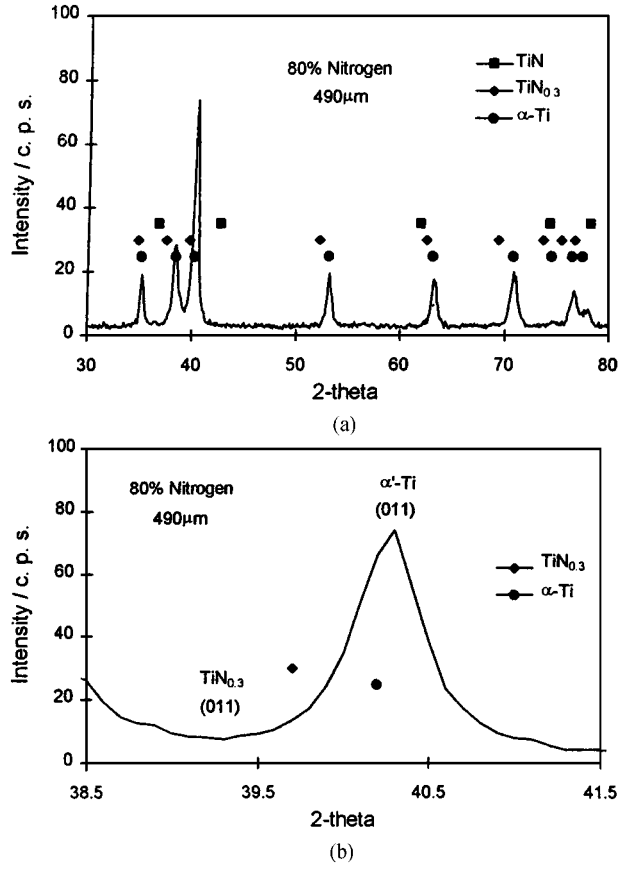

Figure 5 (a) X-Ray Diffraction Spectra at a depth of 490 μm of a laser nitrided Ti alloy. (b) Details of (011) peaks of $TiN_{0.3}$ and α'Ti phases.

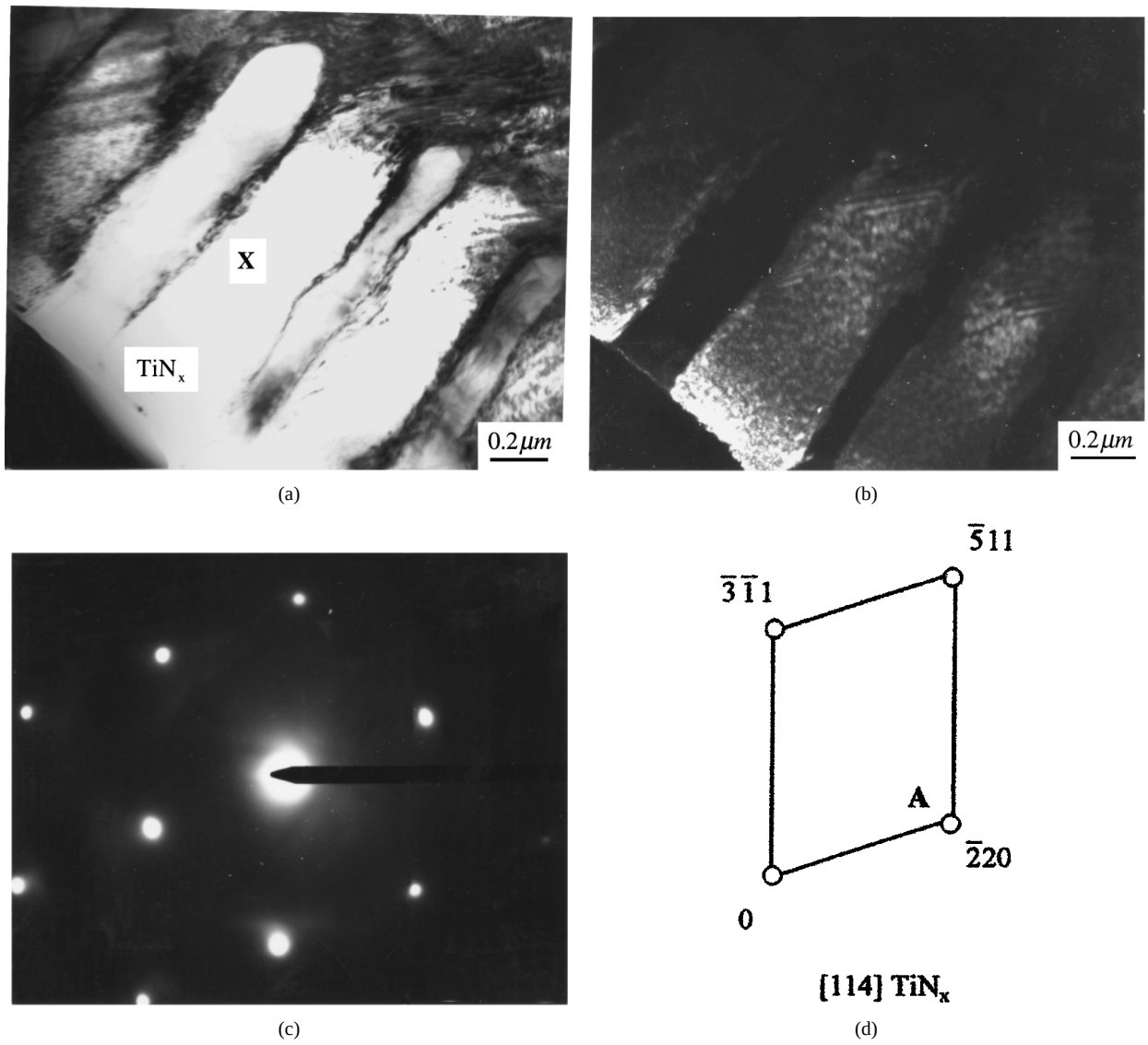

Figure 6 TEM micrographs from the top surface of laser nitrided Ti alloy showing fringe contrast: (a) Bright field, (b) dark field, (c) SAED pattern, (d) indexed as [114] ZA of fcc TiN_x.

were indexed respectively, using a three index system, as hcp [021] and a combination of fcc [116] and hcp [452]. It is considered that the grain with no fringes, which was indexed as an hcp structure, corresponded to $TiN_{0.3}$.

Fig. 8 shows transmission electron micrographs from the slices taken from a depth of 50 μm. The BF in Fig. 8a shows a laminated microstructure. DF images from the two phases are shown in Fig. 8b and c and the corresponding SAED was obtained with the aperture over both phases. This was indexed as two hcp patterns, [113] and [151]. The DF was imaged using respectively, the diffracted spots A and B, seen in the SAED pattern. As both spots are part of cross-grating patterns of hcp structures, it is suggested that one is from α' Ti and the other from $TiN_{0.3}$. This is supported by the more detailed BF micrograph in Fig. 9 taken from a similar area to that of Fig. 8c, but at a depth of 195 μm. Here the needle arrangement is clear and the SAED in Fig. 9b is indexed as hcp with d values corresponding to α'Ti. No evidence of any needles was seen in areas such as that in Fig. 7c, which were commonly imaged in the foils taken from the surface and at depths of 50 μm.

4. Discussion

The different microstructures developed by the laser nitriding producing nonequilibrium phases are considered to be due to the effects of solidification rate, cooling rate of the solid, and diffusion of nitrogen. The previous results [11] showed that when a low laser energy input and a high nitrogen environment were used, a high cooling rate in the solidification stage of the material and a high concentration of nitrogen on the liquid surface, would be expected. Although the temperature at the surface was the highest in the melt, the liquid at the surface could have the highest undercooling, because of the high concentration of nitrogen in the surface liquid whenever the surface temperature was below the melting point of TiN (2930°C) [19].

A spinning laser beam produced a wider melt zone than that produced under corresponding laser processing conditions using a stationary beam [8]. However, a consequence of spinning, which may give a similar result to an oscillating beam, is that the energy density is considerably lower than that obtained from a stationary laser beam [8]. So, a higher cooling rate in the specimen processed with a spinning beam provided

a finer dendritic structure than that observed with a stationary beam, and also did not allow sufficient nitrogen to diffuse into the whole melt zone to form dendritic fcc TiN_x. In the specimen processed with a spinning beam, this results in a division of the microstructure into two Zones: Zone 1 (mainly TiN_x) and Zone 2 (mainly α'-Ti).

Fcc TiN is a hard phase and its formation is most important during laser nitriding. It affects significantly the hardness and abrasive wear of the laser nitrided specimens. TiN has a face centred cubic structure with a lattice parameter value of 4.242 A when the ratio of Ti/N is equal to 1 [20]. However,the XRD results [11,12], show that this phase was hypostoichiometric and varied between $TiN_{0.8}$ and $TiN_{0.85}$. Here, for simplicity, it is described as $TiN_{0.8}$. Also in the XRD work, the intensity change of the $TiN_{0.8}$ peaks revealed that the quantity of precipitates on the top surface increases with increasing nitrogen concentration, in agreement with previous work [21, 22]. The spectra obtained from different depths in the melt zone revealed that the quantity of $TiN_{0.8}$ precipitates decreased with depth in Zone 1, and only a small amount of $TiN_{0.8}$ remained in the top region of Zone 2, which cannot be detected by XRD in the rest of Zone 2. This indicates that the faster cooling rate resulted from the lower power input of the spinning laser beam, allowed a significant nitrogen concentration to diffuse only throughout Zone 1, but in most of Zone 2, the $TiN_{0.8}$ concentration is below the detectable limits of XRD. Furthermore, it is noted that the presence of the dendritic structures, observed by optical microscopy and SEM and shown in Fig. 1, are dependent on the formation of the $TiN_{0.8}$ phase. This strongly suggests that the dendritic structures invariably noted in the laser nitriding literature, is the fcc TiN_x phase, x, may vary with both the nitrogen concentration and the processing conditions.

The present XRD results confirmed the presence of a phase with a lower nitrogen content than $TiN_{0.8}$ as $TiN_{0.3}$ [11, 12, 16]. This phase has been identified previously in thin films made by PVD and CVD methods [17, 18]. Recent work investigating nitriding of CP Ti and a Ti-Al-V alloy, used quantitative microanalysis from EDX in a TEM, to tentatively establish the identity of a similar phase as α-$TiN_{0.25}$ [9]. In the present work, the ($TiN_{0.3}$/TiN_x) intensity ratio change showed that the quantity of $TiN_{0.3}$ precipitates on the top surface increased with increasing nitrogen concentration [11, 12]. The spectra obtained from different depths in the melt zone showed that $TiN_{0.3}$ precipitates formed in Zone 1 and not in Zone 2, or the concentration in Zone 2 was lower than the XRD detection limit. These observations are similar to those discussed above for $TiN_{0.8}$ formation during laser nitriding. They suggest that the existence of $TiN_{0.3}$ phase is very dependent on the diffusion of nitrogen in the melt zone, again in agreement with the previous work on TiN thin films produced by CVD processing [17, 18].

The intensity ratio (α'-Ti/$TiN_{0.8}$) change revealed that the quantity of α'-Ti on the top surface decreased with increasing nitrogen concentration [11, 12]. The spectra obtained from different depths in the melt zone showed that α'-Ti was the only phase formed in the majority of regions of Zone 2. This observation suggests that the needle-like structure in Zone 2, observed by optical microscope and SEM, and shown in Fig. 1, is α'-Ti phase. This has also been noted in the laser nitriding literature [for example, 3, 4, 24]. During the laser nitriding process, the lattice parameters of α'-Ti phase are affected by both the rapid cooling rate and the nitrogen concentration.

The three phases observed by TEM from three distinct morphologies, that is grains/dendrites exhibiting fringes, grains/laths with no fringes, and needles, were very difficult to photograph in a contrast which imaged these three phases in the same area. All three morphologies were very common. The grains containing fringes, and corresponding to fcc TiN, are considered to match the $TiN_{0.8}$-$TiN_{0.85}$ phase identified by X-ray diffractometry. The fringes are considered to be stacking fault fringes. None of the fcc SAED patterns contained spots which fitted a twin pattern.

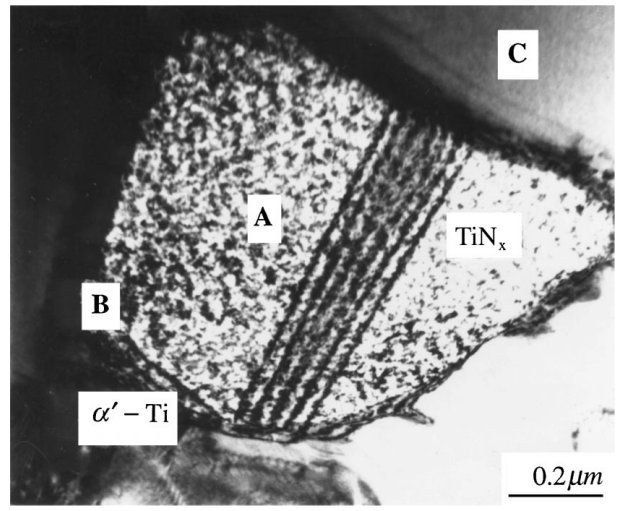

(a)

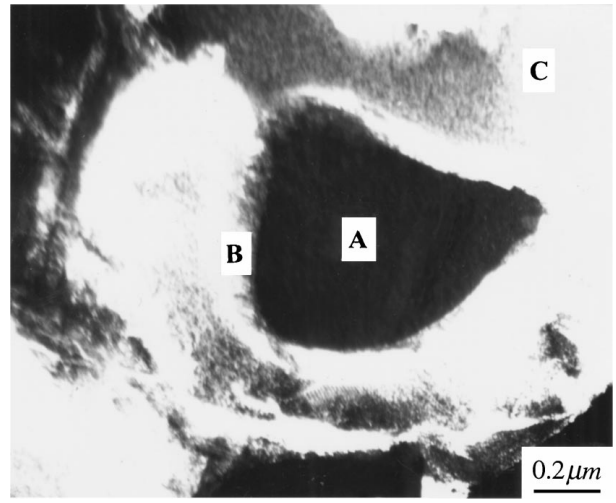

(b)

Figure 7 TEM micrographs from the top surface of laser nitrided Ti alloy showing a grain A with fringe contrast, grain C with no fringe contrast, and B the interface between A and B. (a) Bright field, (b) dark field, (c) SAED patterns from areas A, B, and C and indexed SAED patterns.

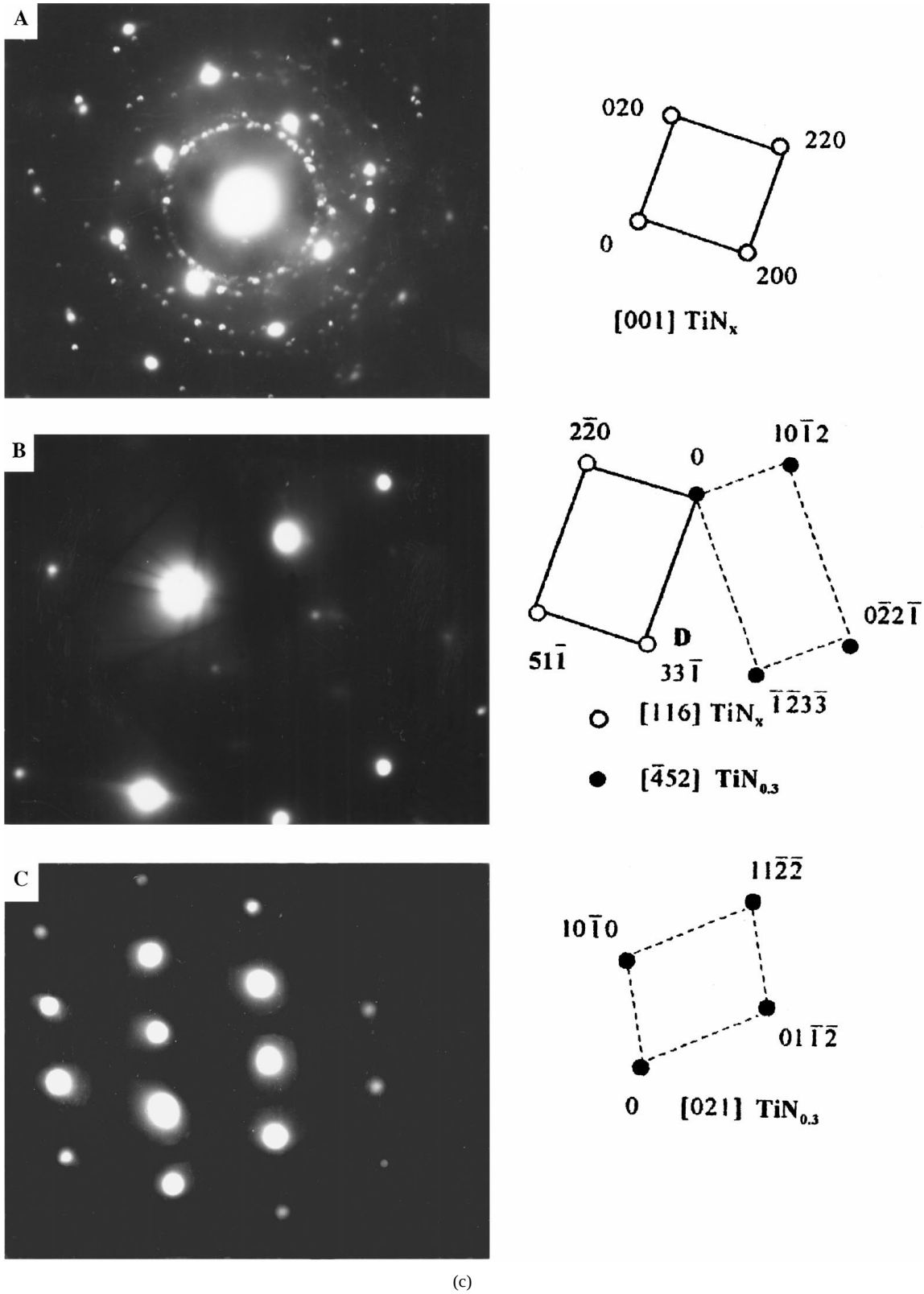

(c)

Figure 7 (*Continued.*)

A recent paper by Yakubtsov *et al.* [25] reviewed the literature on the influence of nitrogen on the stacking fault energy of fcc iron base alloys. They udertook a theoretical study of this effect and related calculated data to that obtained by experiment. They found that the probability of stacking faults occurring initially decreased with an increase in nitrogen concentration, but then rapidly increased. Thus a variation in stacking fault energy in fcc structures, as a function of nitrogen concentration is known.

The observation of stacking fault fringes in the present work, where a concentration of 80% N was used, differs from that in a parallel study by Soib [26], on the laser nitriding of Ti-6Al-4V alloy under similar processing conditions, but using 20% N. Here no fringes were seen on grains which had fcc SAED patterns giving a lattice parameter of 4.24 A. This preliminary result suggests that increasing nitrogen from 20 to 80 atomic percent, decreases the stacking fault energy of Ti-6Al-4V alloy. The faulting may also be related to

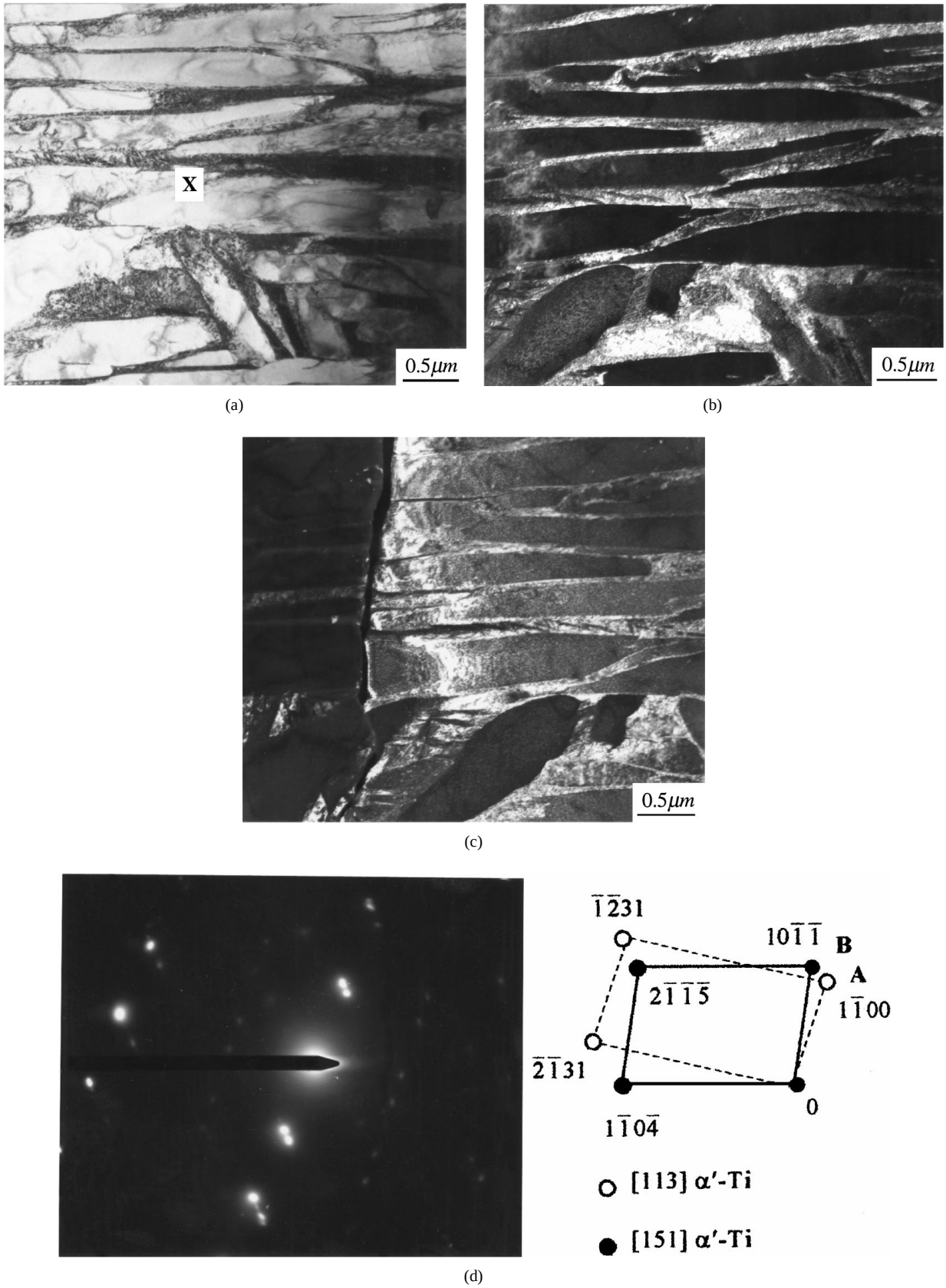

Figure 8 TEM micrographs from a depth of 50 μm, Zone1, from a laser nitrided Ti alloy showing a lath structure. (a) Bright field, (b) dark field using spot A, (c) dark field using spot B with SAED patterns indexed as $TiN_{0.3}$ and α'Ti phases.

the stresses induced by the rapid solidification of the high nitrogen concentration laser nitrided specimens.

The $TiN_{0.3}$ phase, identified in the X-ray patterns and the XPS spectra, frequently within 50 μm of the surface, had similar morphologies when observed in the TEM to the $TiN_{0.8}$ phase, that is laths with rounded ends which are often referred to as dendrites, laths with more angular ends, and quasi-spherical sections. None of these features, which produced hcp SAED patterns with lattice parameters similar to α'Ti, was ever imaged with a set of fringes. The absence of this contrast was used as an indication on the TEM screen, that the

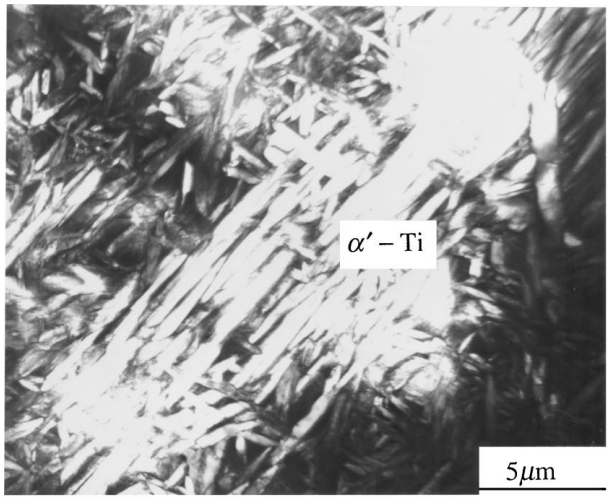

(a)

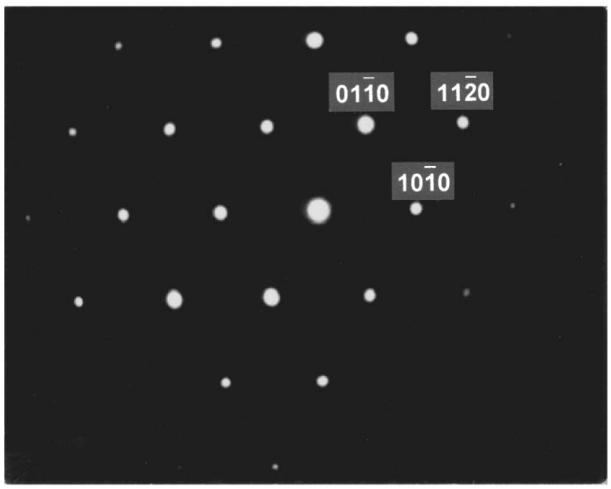

(b)

Figure 9 TEM micrograph from a depth of 190 μm, Zone 2, from a laser nitrided Ti alloy. (a) Bright field of a needle structure, (b) SAED pattern indentified as the α'Ti phase.

phase was likely to be the $TiN_{0.3}$ phase. The matrix phase with the needle morphology, was designated as the martensitic α'Ti phase. This needle phase increased in volume from the surface to a depth of 195 μm, in agreement with the X-ray results.

The question of the concentration of nitrogen in solid solution has been examined by Bars *et al.* [27]. Using their data, (summarized in Fig. 22 of their paper [27]), and making an allowance of 200 Hv for the difference of the hardness of CPTi and Ti-6Al-4V, both without nitrogen, in the present work it is estimated that the α'Ti phase at the top of Zone 2 contains $\sim$4% N in solid solution, while at the bottom of Zone 2, at the melt zone/HAZ interface, there is $<$1% N in solid solution. This estimate does not take into account any influence on hardness of residual stress.

5. Conclusions

1. A microstructural study of the phases developed during the laser nitriding of a Ti-6Al-4V alloy, using a CL5 continuous CO_2 laser with a spinning beam and concentration of 80% nitrogen, was undertaken.

2. The vertical sections perpendicular to the melt track were examined by optical microscopy and SEM, while specimens for XRD, XPS and TEM, were taken parallel to the melt track. In this way, the variation in microstructure as a function of depth from the laser treated surface, was studied.

3. Two zones were identified. Zone 1, within 50 μm of the surface, contained well defined dendrites of fcc $TiN_{0.8}$, plus hcp $TiN_{0.3}$ and hcp α'. Zone 2 consisted of needles of hcp α'. From a consideration of the hardness profiles in Zone 2, it is suggested that at the top of the zone, the α' phase is, in fact, a solid solution containing 3–4% N, which decreased to $<$1% N at the bottom of the zone.

4. The TEM/SAED study showed that the fcc$TiN_{0.8}$ contained fringes, which were considered to be stacking fault fringes. These may be associated with the high nitrogen concentration used for the laser nitriding in this work.

Acknowledgements

Thanks are due to DERA (formerly MOD/RAE) and Imperial Metals Industries, now TIMET, for the gift of materials, to Dr. J.H.P.C. Megaw and his staff, formerly of the Beam Science and Technology Department of AEA Technology, for advice on laser processing. HX acknowledges the award of ORS grant.

References

1. P. H. MORTON, T. BELL, A. WEISHEIT, B. L. MORDIKE and K. SAGOO, Surface Modification Technologies V, Proc. of 5th Int. Conf., edited by T. S. Sudarshan and J. F. Braza (Inst. Mat, London, 1992) p. 593.
2. C. W. DRAPER and J. M. POATE, *Int. Met. Rev.* **30** (1985) 85.
3. S. KATAYAMA, A. MATSUNAWA, A. MORIMOTO, S. ISHIMOTO and Y. AVATA, Proc. Int. Conf. Applied Laser Electro-optics 1983, Laser Inst. of America, p. 127.
4. T. BELL, H. W. BERGMANN, J. LANAGAN, P. H. MORTON and A. M. STAINES, *Surf. Eng.* **2** (1986) 133.
5. H. S. UBHI, T. N. BAKER, P. HOLDWAY and A. W. BOWEN, Proc. 6th World Conf. On Titanium, edited by P. Lacombe, R. Tricot and G. Beranger (Les Editions de Physique, Paris **3**, 1988) p. 1687.
6. V. M. WEERASIHGE, D. R. F. WEST and M. CZAJLIK, *Mat. Sci. Forum* **102/104** (1992) 401.
7. S. MRIDHA and T. N. BAKER, *Mat. Sci. and Eng.* **A188** (1994) 229.
8. H. XIN, S. MRIDHA and T. N. BAKER, *J. of Mat. Sci.* **31** (1996) 22.
9. A. I. P. NWOBU, R. D. RAWLINGS and D. R. F. WEST, *Acta Mater.* **47** (1999) 631.
10. S. Z. LEE and H. W. BERGMANN, Proc. 6th World Conf. on Titanium, edited by P. Lacombe, R. Tricot and G. Beranger (Les Editions de Physique, Paris **3**, 1988) p. 1811.
11. C. HU, H. XIN, L. M. WATSON and T. N. BAKER, *Acta Mater.* **45** (1997) 4311.
12. H. XIN, L. M. WATSON and T. N. BAKER, *ibid.* **46** (1998) 1949.
13. R. HUTCHINGS, *Mater. Lett* **1** (1983) 137.
14. M. K. HIBBS, B. O. JOHANSSON, J. E. SUNDGREN and U. HELMERSSON, *Thin Solid Films* **122** (1984) 115.
15. M. K. HIBBS, J. E. SUNDGREN, B. E. JOHANSSON and B. O. JOHANSSON, *Acta Metall.* **33** (1985) 797.
16. C. HU, S. MRIDHA, H. S. UBHI, P. HOLDWAY, A. W. BOWEN and T. N. BAKER, Proc. 8th Int. Conf. on Titanium, Vol. 3, edited by P. A. Blenkinsop, W. J. Evans and H. W. Flower, *Inst. Mat.* (London, 1995) p. 1959.

17. J. E. SUNDGREN, *Thin Solid Films* **128** (1985) 21.
18. W. LENGAUER and P. ETTMAYER, *Mater. Sci. Eng.* **105/106** (1988) 257.
19. R. C. WEAST and M. J. ASTLE (eds.), Handbook of Chemistry and Physics 61st Edn. (CRC Press, Boca Raton, F1, 1980).
20. H. A. WRIEDT and J. L. MURRAY, in "Phase Diagrams of Binary Titanium Alloys," edited by J. L. Murray (ASM International, Metals Park, OH, USA, 1987) p. 176.
21. B. L. MORDIKE, "Laser Gas Alloying," edited by C. W. Draper and P. Mazzoldi (Maritinus Nijhoff, Dordrecht, NL, 1986) p. 389.
22. S. YERRAMAREDDY and S. BAHADUR, *Wear* **157** (1992) 245.
23. S. SANTUCCI, L. LOZZI, M. PASSACANTANDO, P. PICOZZI, R. ALFONSETTI and R. DIAMANTI, *Thin Solid Films* **290/291** (1996) 376.
24. A. B. KLOOSTERMAN and J. TH. M. DE HOSSON, *J. Mat. Sci.* **32** (1997) 6201.
25. I. A. YAKUBTSOV, A. ARIAPOUR and D. D. PEROVIC, *Acta mater* **47** (1999) 1271.
26. M. S. B. Selamat, PhD. Thesis, University of Strathclyde, Glasgow, U.K., 1999.
27. J-P BARS, E. ETCHESSAHAR and J. DEBUIGNE, *J. Less Comm. Met.* **52** (1977) 51.

Received 12 April
and accepted 19 August 1999